Direct Dynamics Study on the Hydrogen Abstraction Reaction $PH_3 + H \rightarrow PH_2 + H_2$

Xin Yu,* Shen-Min Li, Jing-Yao Liu, Zhen-Feng Xu, Ze-Sheng Li, and Chia-Chung Sun

Institute of Theoretical Chemistry, State Key Laboratory of Theoretical and Computational Chemistry, Jilin University, Changchun 130023, P. R. China

Received: February 1, 1999; In Final Form: June 5, 1999

The hydrogen abstraction reaction $PH_3 + H \rightarrow PH_2 + H_2$ has been studied using an ab initio direct dynamic method. The optimized geometries and frequencies were calculated at the UQCISD/6-311+G** level for the reactant, products, and transition state, as well as 12 points along the minimum energy path. In order to obtain more reliable energies, the single-point calculations were carried out at the G2//QCISD level. The potential barriers obtained for the forward and reverse reactions are 3.24 and 25.99 kcal/mol, respectively. Reaction rate constants and activation energies were calculated for the temperature range 200−1600 K by the canonical variational transition state theory incorporating a small-curvature tunneling correction, and they are in satisfactory agreement with the available experimental values over the measured temperature ranges.

Introduction

The hydrogen abstraction reaction of H with phosphine

$$PH_3 + H \rightarrow PH_2 + H_2$$

has been the subject of many experimental studies. It plays an important role in the gas-phase chemistry of the metal−organic chemical vapor deposition processes used in the manufacture of III−V semiconductor materials[1] and P-doped Si and Ge films.[2] It is also thought to be involved in forming the trace amounts of PH_3 found in the atmospheres of Jupiter and Saturn. Lee et al.[3] made the first determination of the absolute rate constants for this reaction over the temperature range 209−495 K, and they predicted that the hydrogen abstraction reaction might occur in the atmospheres of Jupiter and Saturn. Alexsandrov et al.[4] measured a room temperature rate constant. Recently, Arthur and Cooper[5] also measured rate constants in the temperature range 293−472 K, and combined their results with those of Lee et al.[3] to give a best value for the rate constants over the temperature range 200−500 K of $k = (7.21 \pm 0.41) \times 10^{-11} \exp[(-887 \pm 19)/T]$ cm^3 s^{-1}. However, to our knowledge, little theoretical attention has been paid to this reaction.

In this paper, an attempt is made to investigate theoretically the dynamic properties of the hydrogen abstraction reaction. Ab initio calculations have been performed to obtain electronic structure information, including geometries, energies, gradients, and force constants at the selected points along the minimum energy path. In addition, the variational transition state theory incorporating a small-curvature tunneling correction method (CVT/SCT) has been employed to obtain the reaction rate constants and activation energies in the temperature range 200−1600 K. They are in satisfactory agreement with the available experimental results. Also, the calculated result shows that the forward reaction is favored over the reverse reaction.

Calculation Methods

By means of the *Gaussian 94* program,[6] high level ab initio calculations were carried out. First, equilibrium geometries and frequencies of the stationary points (reactant, products, and transition state) were calculated at the UQCISD/6-311+G** level. At the same level, the minimum energy path (MEP) was obtained by the intrinsic reaction coordinate theory (IRC) with a gradient step size of 0.05 (amu)$^{1/2}$ bohr. Furthermore, at 12 selected points (6 points in the reactant channel, 6 points in the product channel) along the MEP, the force constant matrices as well as the harmonic vibrational frequencies were obtained. Because the shape of the MEP is important for the calculation of rate constants, the energies of the MEP were refined by the G2//QCISD method,[7] which applies the G2 method[8] at the UQCISD stationary point geometries and along the UQCISD reaction path. Note that the G2 calculation in this paper is made with UQCISD/6-311+G** geometries and frequencies rather than the prescribed UMP2/6-31G* geometries and UHF/6-31G* frequencies. Finally, the POLYRATE 7.4 program[9] was used for the calculation of theoretical rate constant and activation energy. For the purpose of comparison, the conventional transition state theory (TST) and the canonical variational transition state theory (CVT) as well as the CVT incorporating a small-curvature tunneling correction method (CVT/SCT) proposed by Truhlar and co-workers[10,11] were performed to determine the reaction rate constants and activation energies. The rate constants were calculated at 23 temperatures and the activation energies are computed for seven temperature pairs using mass-scaled Cartesian coordinate. The Euler single-step integrator with a step size of 0.0001 (amu)$^{1/2}$ bohr was used to follow the MEP, and the generalized normal mode analysis was performed every 0.01 (amu)$^{1/2}$ bohr. The curvature components were calculated using a quadratic fit to obtain the derivative of the gradient with respect to the reaction coordinate. This is an example of the direct dynamic method[12] since rate constants are obtained without fitting the electronic structure data to an analytic potential energy surface.

Results and Discussion

A. Stationary Points. The optimized geometric parameters of the reactant (PH_3), products (PH_2 and H_2), and transition state at the UQCISD/6-311+G** level are shown in Figure 1. The optimized geometric parameters of the reactant and products are in good agreement with the experimental data.[13,14] From

10.1021/jp990367u CCC: $18.00
Published on Web 07/27/1999

TABLE 1: Harmonic Vibrational Frequencies (cm^{-1}) and Zero-Point Energies (ZPE) (kcal/mol) at the UQCISD/6-311+G Level**

	PH_3	H_2	PH_2	TS
	$\gamma_{r1}(A_1)^a$ 2465(2329)^b	γ_{p1} (Σ_g^+) 4419(4403)	$\gamma_{p2}(B_2)$ 2438(2310)	$\gamma_1(A')$ 2460
	$\gamma_{r2}(E)$ 2460(2328)		$\gamma_{p3}(A_1)$ 2432(2310)	$\gamma_2(A'')$ 2455
	$\gamma_{r3}(E)$ 1154(1121)		$\gamma_{p4}(A_1)$ 1156(1101)	$\gamma_3(A')$ 1458
	$\gamma_{r4}(A_1)$ 1051(990)			$\gamma_4(A')$ 1137
				$\gamma_5(A'')$ 1117
				$\gamma_6(A')$ 1016
				$\gamma_7(A')$ 381
				$\gamma_8(A'')$ 376
				$\gamma_9(A')$ 1182*i*
ZPE	15.37	6.32	8.62	14.87

[a] γ_r, the vibrational frequency of reactant; γ_p the vibrational frequency of product; γ the vibrational frequency of TS. [b] The values in parentheses are experimental values (ref 15 for PH_3, ref 16 for PH_2, and ref 17 for H_2).

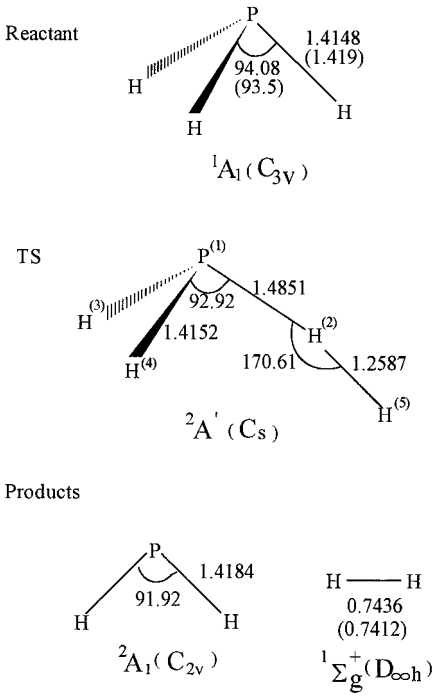

Figure 1. Geometric parameters (in angstroms and degrees) of the stationary points at the UQCISD/6-311+G** level. The numbers in parentheses are experimental values.[13,14]

these results, we might infer that the same accuracy can be expected for calculated transition state geometries. In the transition state structure, the length of bond $P^{(1)}-H^{(2)}$ which will be broken increases by 5% with respect to the equilibrium bond length of PH_3. The length of the $H^{(2)}-H^{(5)}$ bond that will form hydrogen molecule is 1.7 times as large as the equilibrium bond length of the hydrogen molecule. Therefore, the transition state structure is reactantlike, and the hydrogen abstraction reaction will proceed via an early transition state.

Table 1 gives the harmonic vibrational frequencies and zero-point energies (ZPE) of the reactant, products, and transition state at the UQCISD/6-311+G** level, as well as the corresponding experimental results.[15−17] It is shown that the calculated frequencies of the reactant and products are slightly larger than those of the experimental values, and the maximum error between them is about 6%. The transition state has only one imaginary frequency.

The reaction enthalpy and potential barrier are listed in Table 2. The calculated reaction enthalpies at temperature 298 K with respect to G2//QCISD and UQCISD with ZPE correction methods are −23.06 and −21.61 kcal/mol, respectively, therefore, the forward reaction is exothermic. The calculated reaction

TABLE 2: Reaction Enthalpy (ΔH^0_{298}), Forward (ΔE^f) and Reverse (ΔE^r) Potential Barriers (kcal/mol)

	G2//QCISD[a]	UQCISD (ZPE)[a]	Expt.
ΔH^0_{298}	−23.06	−21.61	−23.09
ΔE^f	3.24	4.18	
ΔE^r	25.99	27.83	

[a] Total energies (in hartrees) at UQCISD (ZPE): PH_3, −342.615710; H, −0.499810; PH_2, −341.994942; H_2, −1.158274; TS, −343.108866. At G2//QCISD: PH_3, −342.677948; H, −0.50; PH_2, −342.048462; H_2, −1.165751; TS, −343.172791.

enthalpy at the G2//QCISD level is much closer to the experimental value, −23.09 kcal/mol, which is obtained by the experimental standard heats of formation (PH_3, 1.32 kcal/mol;[18] H, 51.90 kcal/mol;[18] PH_2, 30.13 kcal/mol;[19] H_2, 0.0 kcal/mol). Table 2 also shows that, for the forward reaction, the potential barriers obtained by G2//QCISD and UQCISD with ZPE correction methods take the values 3.24 and 4.18 kcal/mol, respectively. The reverse reaction potential barrier is calculated at the G2//QCISD level to give 25.99 kcal/mol. Since the forward barrier is far smaller than the reverse barrier, we expect that the forward reaction is favored over the reverse reaction.

B. Reaction Path Properties. The minimum energy path (MEP) is calculated at the UQCISD/6-311+G** level by the intrinsic reaction coordinate theory from the transition state to the reactants and products, respectively. The energies of MEP are refined by G2//QCISD method, and the maximum value for the $V_{MEP}(s)$ at G2//QCISD level corresponds to the saddle point structure at QCISD/6-311+G** level. The changes of generalized normal mode vibrational frequencies along the MEP at UQCISD/6-311+G** level as functions of the intrinsic reaction coordinate *s* are shown in Figure 2. It should be pointed out that, in the negative limit of *s*, the frequencies are associated with the reactant (PH_3), and in the positive limit of *s*, the frequencies are associated with the products (PH_2 and H_2). Now let us limit our discussion to the frequencies in the vicinity of the transition state. Near the transition state ($s = 0$), there are eight vibrational frequencies, of which three frequencies keep unchanged during the whole reaction process. Note that two of the three vibrational modes (modes 1 and 2) correspond to the degenerate stretching vibrations of $P^{(l)}-H^{(3)}$ and $P^{(l)}-H^{(4)}$, and the remaining one (mode 4) is of the bending vibration of $H^{(3)}-P^{(1)}-H^{(4)}$. In the whole process, the invariable character of the three vibrational modes indicates that the $H^{(2)}$ abstraction has almost no influence on the vibrations associated with the bending of $H^{(3)}-P^{(1)}-H^{(4)}$ and the stretching of $P^{(1)}-H^{(3)}$ and $P^{(1)}-H^{(4)}$. In the process of the reaction, the frequency of mode 3 has a significant change in the region from about $s = -0.5$ to 0.8 $(amu)^{1/2}$ bohr, because it connects the frequency of the $P^{(1)}-H^{(2)}$ stretching vibration of PH_3 with the frequency of the

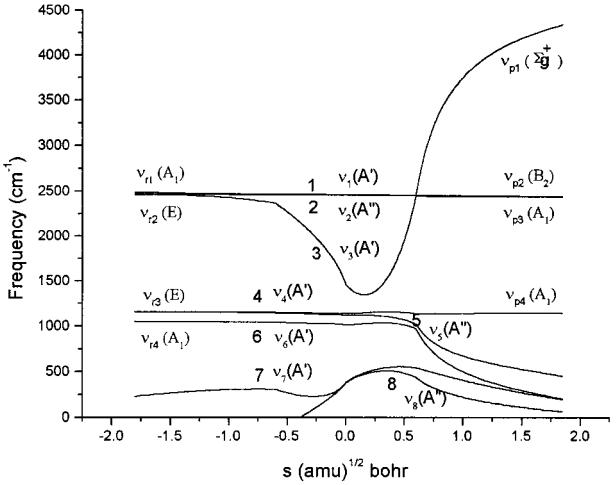

Figure 2. Changes of the generalized normal-mode vibrational frequencies as functions of s (amu)$^{1/2}$ bohr at the UQCISD/6-311+G** level.

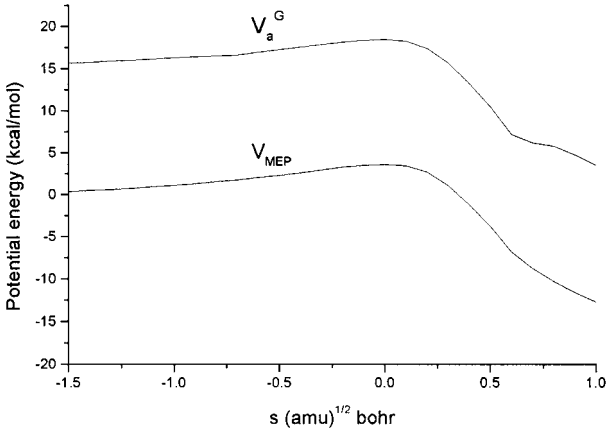

Figure 3. Classical potential energy (V_{MEP}) and ground-state adiabatic potential energy (V_a^G) as functions of s (amu)$^{1/2}$ bohr.

$H^{(2)}-H^{(5)}$ stretching vibration of H_2. Therefore, mode 3 can be referred to as the "reaction mode". Frequencies of modes 5 and 6, which are of bending vibrations with respect to $H^{(2)}-P^{(1)}-H^{(3)}$ and $H^{(2)}-P^{(1)}-H^{(4)}$, decrease gradually accompanying the breaking of bond $P^{(1)}-H^{(2)}$. The remaining vibrational modes 7 and 8 turn into translation or rotation in both the reactant region and product region.

The classical potential energy $V_{MEP}(s)$ and the ground-state adiabatic potential energy $V_a^G(s)$ along the MEP as functions of the intrinsic reaction coordinate s are depicted in Figure 3. It can be seen that the positions of maximum value for the $V_{MEP}(s)$ and $V_a^G(s)$ curves are nearly the same, and it implies that the variational effect for the calculation of rate constants is small. For a deeper understanding of the variational effect, the dynamic bottleneck properties of the reaction are listed in Table 3. It is shown that the positions s of the variational transition state at various temperatures deviate from the saddle point at $s = 0$. The deviation is largest at 1600 K, where it is 0.1472 (amu)$^{1/2}$ bohr, and the corresponding V_{MEP} and V_a^G are 3.22 kcal/mol and 17.97 kcal/mol, respectively. Since, for the classical transition state ($s = 0$), V_{MEP} and V_a^G take the values 3.62 kcal/mol and 18.48 kcal/mol, respectively, the largest deviations, V_a^G ($s = 0.1472$) $- V_a^G$ ($s = 0$) $= -0.51$ kcal/mol and V_{MEP} ($s = 0.1472$) $- V_{MEP}$ ($s = 0$) $= -0.40$ kcal/mol, are not large. Thus the variational effect for the calculation of rate constant is small.

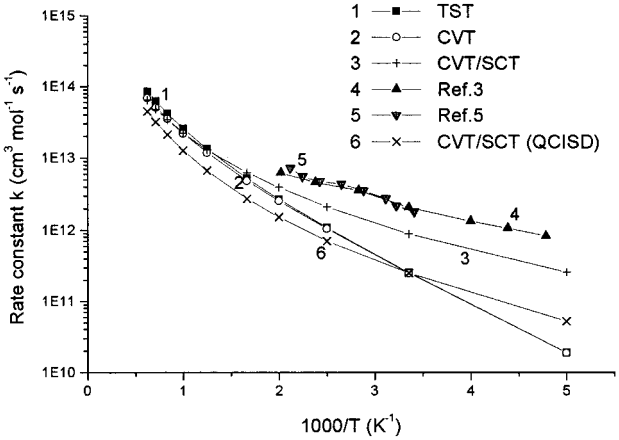

Figure 4. Forward reaction rate constants k (cm3 mol^{-1} s^{-1}) as functions of the reciprocal of the temperature (K^{-1}) over the temperature range 200−1600 K.

TABLE 3: Bottleneck Properties of Reaction (Based on CVT Method)

T (K)	s (amu)$^{1/2}$ bohr	V_{MEP} (kcal/mol)	V_a^G (kcal/mol)
S.P.	0.0000	3.62	18.48
0.00	0.0044	3.62	18.49
200.00	0.0073	3.61	18.48
298.00	0.0169	3.61	18.48
400.00	0.0308	3.60	18.47
500.00	0.0501	3.57	18.43
600.00	0.0718	3.52	18.37
800.00	0.1067	3.40	18.22
1000.00	0.1284	3.31	18.10
1200.00	0.1445	3.23	18.00
1400.00	0.1462	3.22	17.99
1600.00	0.1472	3.22	17.97

Rate Constant Calculation

For the purpose of comparison, calculations by means of the conventional transition state theory (TST), the canonical variational transition state theory (CVT), and the CVT incorporating a small-curvature tunneling correction method (CVT/SCT) were performed for obtaining the reaction rate constants and activation energies in the temperature range 200−1600 K. The TST rate constants (line 1), the CVT rate constants (line 2), the CVT/SCT rate constants (line 3), and the experimental results (lines 4 and 5) of the forward reaction are plotted against the reciprocal of temperature in Figure 4. It is seen that the rate constants of TST (line 1) and CVT (line 2) are nearly the same in the whole temperature range 200−1600 K. This enables us to conclude that the variational effect for the calculation of rate constant is small. It should be noted that the rate constants of TST and CVT deviate substantially from the experimental values[3,5] over the measured temperature range 209−495 K, whereas the CVT/SCT rate constants (line 3) are in much better agreement. Table 4 lists the forward reaction rate constants for the temperature range 200−1600 K. From it we can see that the values of the rate constant calculated by the TST, CVT, and CVT/SCT methods at 209 K are lower than the corresponding experimental values by a factor of 97%, 97%, and 57%, respectively. At 495 K, the factor is 58%, 60% and 34% respectively. This indicates that the small-curvature tunneling correction is important in the calculation of the rate constant in the lower temperature range. Furthermore, Figure 4 shows that in the temperature range 500−1600 K, the rate constants of TST (line 1), CVT (line 2), and CVT/SCT (line 3) are nearly the same, and this means that the small-curvature tunneling (SCT) correction is very small in the higher temperature range. The rate constants of CVT/SCT at

TABLE 4: Forward Reaction Rate Constants (cm^3 mol^{-1} s^{-1}) for the Temperature Range 200−1600 K

	TST	CVT	CVT/SCT	Ref 3	Ref 5
200	1.88*10^{10}	1.87*10^{10}	3.11*10^{11}		
209	2.63*10^{10}	2.62*10^{10}	3.53*10^{11}	8.25*10^{11}	
228	4.90*10^{10}	4.88*10^{10}	4.57*10^{11}	1.07*10^{12}	
250	9.03*10^{10}	8.97*10^{10}	6.00*10^{11}	1.33*10^{12}	
293	2.31*10^{11}	2.29*10^{11}	9.57*10^{11}		1.79*10^{12}
298	2.53*10^{11}	2.51*10^{11}	1.01*10^{12}	2.08*10^{12}	
310	3.14*10^{11}	3.11*10^{11}	1.13*10^{12}		2.15*10^{12}
321	3.76*10^{11}	3.72*10^{11}	1.25*10^{12}		2.73*10^{12}
347	5.56*10^{11}	5.49*10^{11}	1.56*10^{12}		3.52*10^{12}
353	6.02*10^{11}	5.97*10^{11}	1.64*10^{12}	3.57*10^{12}	
377	8.25*10^{11}	8.13*10^{11}	1.97*10^{12}		4.33*10^{12}
400	1.08*10^{12}	1.05*10^{12}	2.33*10^{12}		
412	1.22*10^{12}	1.20*10^{12}	2.52*10^{12}		4.70*10^{12}
445	1.69*10^{12}	1.65*10^{12}	3.11*10^{12}		5.53*10^{12}
472	2.14*10^{12}	2.08*10^{12}	3.62*10^{12}		7.22*10^{12}
495	2.58*10^{12}	2.50*10^{12}	4.09*10^{12}	6.20*10^{12}	
500	2.68*10^{12}	2.59*10^{12}	4.20*10^{12}		
600	5.21*10^{12}	4.92*10^{12}	6.50*10^{12}		
800	1.32*10^{13}	1.19*10^{13}	1.25*10^{13}		
1000	2.54*10^{13}	2.16*10^{13}	2.04*10^{13}		
1200	4.16*10^{13}	3.38*10^{13}	3.03*10^{13}		
1400	6.20*10^{13}	4.85*10^{13}	4.35*10^{13}		
1600	8.55*10^{13}	6.56*10^{13}	5.91*10^{13}		

TABLE 5: Activation Energies (kcal/mol) for $PH_3 + H \rightarrow PH_2 + H_2$

T range (K)	TST	CVT	CVT/SCT
200−298	3.14(4.20)[a]	3.13(4.16)	1.42(1.97)
298−400	3.36(4.41)	3.33(4.33)	1.95(2.58)
400−500[b]	3.64(4.70)	3.58(4.57)	2.35(3.13)
500−600	3.96(5.01)	3.82(4.87)	2.63(3.65)
600−800	4.45(5.51)	4.19(5.41)	3.09(4.41)
800−1600	5.93(6.99)	5.45(6.81)	4.96(6.13)

[a] Values in parentheses are obtained at the QCISD/6-311+G** level of theory. [b] To 209−495 K, the activation energy in kcal/mol is 1.47 in ref 3, 1.76 in ref 5, 2.38 at QCISD/6-311+G** level, and 1.76 at G2//QCISD level in this work.

QCISD/6-311+G** level (line 6) are also plotted in Figure 4. Obviously, they are not in agreement with the experimental values in comparison with the rate constants of CVT/SCT at G2//QCISD level. Table 5 reports Arrhenius activation energies as a function of temperature for several two-temperature fits to the theoretical results. In parentheses are the values obtained at QCISD/6-311+G** level. It is apparent that the activation energy gets larger with the increase of temperature, and the G2//QCISD value of 209−495 K is in satisfactory agreement with the available experimental value. By the comparison between theoretical and experimental rate constants and between theoretical and experimental activation energies, it is not difficult to find that the G2//QCISD method is more reliable than the QCISD/6-311+G** method for this reaction. The rate constants of the reverse reaction are insignificant, thus the reverse reaction is difficult to proceed.

Conclusion

In this work, the hydrogen abstraction reaction $PH_3 + H \rightarrow PH_2 + H_2$ has been investigated theoretically. From the above discussion, the following conclusions can be drawn:

(1) The potential barriers for the forward and reverse reactions, calculated at the G2//QCISD level, are 3.24 and 25.99 kcal/mol, respectively.

(2) By analyzing the changes of generalized normal-mode vibrational frequencies along the reaction path, we find that the "reaction region" is approximately from about $s = -0.5$ to 0.8 $(amu)^{1/2}$ bohr, including the breaking of $P^{(1)}-H^{(2)}$ and the forming of $H^{(2)}-H^{(5)}$.

(3) The reaction rate constants and activation energies are calculated for the temperature range 200−1600 K using the variational transition state theory incorporating a small-curvature tunneling correction. The calculated forward reaction rate constants and activation energies are in satisfactory agreement with the available experimental values[3,5] over the measured temperature range. The calculated results show that the variational effect on the value of the rate constant is small, and that the tunneling correction is important in the calculation of the rate constant in the lower temperature range.

Acknowledgment. The authors thank Professor Donald G. Truhlar for providing the POLYRATE 7.4 program. This work is supported by the National Science Foundation of China.

References and Notes

(1) Stringfellow, G. B. In *Organometallic Vapor-Phase Epitaxy*: *Theory and Practice*; Academic Press: New York, 1989.

(2) Kampas, F. J. In *Semiconductors and Semimetals;* Pankove, J. I., Ed.; Academic Press: New York, 1984; Vol. 21.

(3) Lee, J. H.; Michael, J. V.; Payne, W. A.; Whytock, D. A.; Stief, L. J. *J. Chem. Phys.* **1976**, *65*, 3280.

(4) Alexsandrov, E. N.; Arutyunov, V. S.; Dubroviua, I. V.; Kozlov, S. N. *Fizika Gorentya i Vzryva*, **1982**, *18*, 73.

(5) Arthur, N. L.; Cooper, I. A. *J. Chem. Soc., Faraday Trans.* **1997**, *93*, 521.

(6) Frisch, M. J.; Trucks, G. W.; Schlegel, H. B.; Gill, P. M. W.; Johnson, B. G.; Robb, M. A.; Cheeseman, J. R.; Keith, T.; Petersson, G. A.; Montgomery, J. A.; Raghavachari, K.; Al-Laham, M. A.; Zakrzewski, V. G.; Ortiz, J. V.; Foresman, J. B.; Cioslowski, J.; Stefanov, B. B.; Nanayakkara, A.; Challacombe, M.; Peng, C. Y.; Ayala, P. Y.; Chen, W.; Wong, M. W.; Andres, J. L.; Replogle, E. S.; Gomperts, R.; Martin, R. L.; Fox, D. J.; Binkley, J. S.; Defrees, D. J.; Baker, J.; Stewart, J. P.; Head-Gordon, M.; Gonzalez, C.; Pople, J. A. *Gaussian 94*, Revision E.2, Gaussian, Inc., Pittsburgh, PA, 1995.

(7) Durant, J. L., Jr.; Rohlfing, C. M. *J. Chem. Phys.* **1993**, *98*, 8031.

(8) Curtiss, L. A.; Raghavachari, L.; Trucks, G. W.; Pople, J. A. *J. Chem. Phys.* **1991**, *94*, 7221.

(9) Steckler, R.; Chuang, Y.-Y.; Fast, P. L.; Coitino, E. L.; Corchado, J. C.; Hu, W.-P.; Liu, Y.-P.; Lynch, G. C.; Nguyen, K. A.; Jackels, C. F.; Gu, M. Z.; Rossi, I.; Clayton, S.; Melissas, V. S.; Garrett, B. C.; Isaacson, A. D.; Truhlar, D. G. *POLYRATE* version 7.4; University of Minnesota, Minneapolis, 1997.

(10) Truhlar, D. G.; Isaacson, A. D.; Garret, B. C. In *Theory of Chemical Reaction Dynamics*; Baer, M., Ed.; CRC Press: Boca Raton, FL, 1985; p 65.

(11) Steckler, R.; Hu, W.-P.; Liu, Y.-P.; Lynch, G. C.; Garrett, B. C.; Isaacson, A. D.; Melissas, V. S.; Lu, D.-H.; Troung, T. N.; Rai, S. N.; Hancock, G. C.; Lauderdale, J. G.; Joseph, T.; Truhlar, D. G. *Comput. Phys. Commun.* **1995**, *88*, 341.

(12) Truhlar, D. G.; Gordon, M. S. *Science* **1990**, *249*, 491.

(13) Nielsen, H. H. *J. Chem. Phys.* **1952**, *20*, 759.

(14) Gray, H. B. In *Chemical Bonds;* Benjamin, W. A.: Menlo Park, CA, 1973.

(15) Mc Conaghie, V. M.; Nielsen, H. H. *J. Chem. Phys.* **1953**, *21*, 1836.

(16) In *NIST Chemistry WebBook*, NIST Standard Reference Database Number 69, November 1998 Release. Vibrational frequency data compiled by T. Shimanouchi.

(17) Levine, Ira N. In *Molecular Spectroscopy;* Wiley: NewYork, 1975.

(18) Barin, I.; Knacke, O. *Thermochemical Properties of Inorganic Substances;* Springer-Verlag: Berlin, 1973. Barin, I.; Knacke, O.; Kubashewski, O. *Thermochemical Properties of Inorganic Substances*, Springer-Verlag: Berlin, supplement; 1977.

(19) Chase, M. W., Jr.; Davies, C. A.; Downey, J. R., Jr.; Frurip, D. J.; McDonald, R. A.; Syverud, A. N. JANAF Thermochemical Tables (Third Edition), *J. Phys. Chem. Ref. Data*, Suppl. 1, **1985**, *14*, 1−1856.